

Prompt Photofission Neutron Detection in Depleted Uranium

A.J. Jinia^{1,*}, T.E. Maurer,¹ C.A. Meert,¹ O.V. Pakari,¹ S.D. Clarke,^{1,†} H.S. Kim,²
D.D. Wentzloff,² and S.A. Pozzi^{1,3,‡}

¹*Department of Nuclear Engineering and Radiological Sciences, University of Michigan, 2355 Bonisteel Blvd, Ann Arbor, Michigan 48109-2104, USA*

²*Department of Electrical Engineering and Computer Sciences, University of Michigan, 1301 Beal Ave, Ann Arbor, Michigan 48109-2104, USA*

³*Department of Physics, University of Michigan, 450 Church Street, Ann Arbor, Michigan 48109-1040, USA*

(Received 12 September 2022; revised 28 February 2023; accepted 1 May 2023; published 23 May 2023)

The detection of prompt photofission neutrons during active interrogation is a strong indication of the presence of special nuclear materials. However, the high-energy photons used for interrogation create a very challenging radiation environment for the detection of prompt fission signatures. These challenges include detector saturation and pulse pile-up. Additionally, there is an elevated neutron background that further challenges the detection of prompt fission neutrons. This background is produced because of (γ, Xn) photonuclear reactions in the surrounding high-Z materials. Here, we demonstrate the detection of prompt photofission neutrons in these challenging environments. Depleted uranium (DU) and lead targets are interrogated with bremsstrahlung photons produced by a 9-MV electron linear accelerator. Fast neutrons are detected with *trans*-stilbene organic detectors, and scintillation pulses are analyzed using a previously developed and demonstrated artificial neural network system. We observe a 5 times higher photoneutron count rate when the lead target is replaced with the DU target. Additionally, we observe a difference in the photoneutron light-output distributions of lead and DU. This difference in the measured distributions is due to the difference in the photoneutron-energy spectra; DU photoneutrons are emitted with (γ, n) and watt-energy spectra, whereas lead photoneutrons are emitted with only the (γ, n) spectrum.

DOI: 10.1103/PhysRevApplied.19.054073

I. INTRODUCTION

Photon interrogation systems that rely on prompt photofission signatures are promising for the detection of concealed or hidden special nuclear materials (SNMs) [1, 2]. In such interrogation systems, materials are bombarded with high-energy photons, which induce various photonuclear reactions, such as and photofission, i.e., (γ, f) in SNMs. The prompt fission neutrons produced by photofission reactions are a strong indication of the presence of SNMs. In recent years, significant efforts have been made in the detection of prompt photofission signatures.

In 2007, Blackburn *et al.* successfully exploited the emissions of prompt fission signatures for the detection of shielded nuclear materials [3]. In their experiment, high-energy photons were produced with a 10-MV linear accelerator (linac) from Varitron that was operating at 125 Hz. Interrogation measurements with (a) no material present (active background), (b) bismuth, and (c) depleted uranium were performed and signals that fell under 3 μ s of

the accelerator pulses were analyzed. A fast EJ-200 plastic scintillator detector was used to monitor photoneutrons. The obtained integrated counts demonstrate the successful detection of prompt fission neutrons from depleted uranium as well as (γ, n) photoneutrons from bismuth. In a similar experiment, Clarke *et al.* exploited the differences in the shape of time-of-flight distributions to differentiate depleted uranium from lead [4].

In 2013, Sari *et al.* attempted to detect prompt fission neutrons using a 17-MV linac to produce photoneutrons in a 1-cm-thick tantalum target [5]. These photoneutrons were then used to interrogate ^{235}U and ^{239}Pu samples of varying masses. Three ^3He neutron detectors embedded in polyethylene and surrounded by cadmium were used to measure prompt and delayed fission neutrons. The results obtained showed that both prompt and delayed fission neutron count rates increased with an increase in the mass of ^{235}U and ^{239}Pu samples. Additionally, Sari *et al.* reported the ratio between prompt and delayed fission neutrons. These measured ratios were 31.87 for ^{235}U and 98.54 for ^{239}Pu .

In 2014, Mueller *et al.* proposed a method to discriminate between fissile and nonfissile contents of SNMs [6,7]. The proposed method exploits the difference

*ajinjia@umich.edu

†clarkesd@umich.edu

‡pozzisa@umich.edu

in the prompt neutron yield parallel and perpendicular to the plane of γ -ray- (γ, Xn) photons with energies between 5.3 and 7.6 MeV are used to interrogate several actinide targets (i.e., ^{232}Th , $^{233,235,238}\text{U}$, ^{237}Np , and $^{239,240}\text{Pu}$) and 18 BC-501A liquid scintillators are used for fast-neutron detection. The authors found that nonfissile targets had significant polarization asymmetries ranging from 0.2 to 0.5, whereas fissile targets had asymmetries of nearly zero. The method proposed by Mueller and co-workers can be used to simultaneously detect and identify fissile and nonfissile fissionable material during active interrogation. Since the asymmetry is much smaller for fissile actinides, this method can theoretically be used to determine the enrichment of small samples of SNMs (approximately 1 g/cm²) to the level of 10% enrichment. Additionally, the authors found that this asymmetry was relatively insensitive to moderate amounts of lead, steel, and high-density polyethylene shielding. Another study on the applicability of photofission reaction ratios to identify enrichment was performed by Chin *et al.* and Kimura *et al.* [8,9]. The authors demonstrated that by calculating the ratio of photofission neutrons produced by a higher photon energy over a lower photon energy, quantitative information on uranium enrichment could be obtained.

An x-ray inspection system was developed by Passport Systems Inc. to scan cargo containers for possible contraband, anomalies, and nuclear threats [10,11]. This system utilizes a continuous-wave 9-MeV rhodotron to induce photofission reactions in SNMs. Prompt fission neutrons are detected with phenylxylylethane liquid scintillation detectors. During the initial testing, interrogation measurements with (a) depleted uranium, (b) heavy water, and (c) beryllium are performed. Both heavy water and beryllium have defined photoneutron endpoint energies at 3.4 and 6.5 MeV, respectively, for a 9-MeV interrogating photon. However, depleted uranium does not have an endpoint energy because of the presence of prompt fission neutrons. The x-ray interrogation system developed by Passport Inc. exploits this difference in the energy spectra of photoneutrons to reduce false positives and efficiently identify SNMs.

High-energy x-ray interrogation systems that exist in the literature show promise in the detection and characterization of SNMs. At the University of Michigan, we investigate the use of organic scintillation materials of varying sizes, photomultiplier tubes versus silicon photomultiplier read-out options, and machine learning algorithms for the detection of prompt photofission neutrons. In our previous work, we demonstrated the detection of photoneutrons from depleted uranium using a 9-MV electron linac and 6-mm *trans*-stilbene cubes [12]. Here, we investigate a larger volume of *trans*-stilbene crystals for photoneutron detection and a neural-network-based digital system for scintillation pulse processing. Monte Carlo simulations are performed using the MCNPX-PoliMi transport code [13],

and the measured results are compared with the simulated results.

The structure of this paper is as follows. We begin by describing the theory of active interrogation followed by our experimental setup for the interrogation of depleted uranium and lead targets. We then provide a detailed description of steps performed during the MCNPX-PoliMi simulation. We conclude with a discussion of obtained results and any discrepancies observed between measurement and simulation.

II. THEORY

Electron linacs are commonly used to produce high-energy photons, which are emitted through the bombardment of accelerated electrons on a high-Z x-ray convertor target. These linacs operate in pulsed mode and the pulsed nature of the emitted bremsstrahlung photons facilitates the detection of prompt photofission neutrons without saturating the detection systems. On average, the prompt neutron yields per fission are 2.74 and 2.91 for ^{235}U and ^{238}U isotopes, respectively [14]. This yield of prompt neutrons increases with photon energy [Fig. 1(a)]. The greater yield of prompt photofission neutrons constitutes a strong detection signal. Additionally, the energy spectrum of prompt neutrons is another property of specific interest. Figure 1(b) shows the difference in the energy spectrum of photoneutrons produced by (γ, f) and (γ, n) reactions. Photoneutrons through (γ, n) reactions have a maximum kinetic energy, which is determined by the interrogating photon energy and the reaction's Q value. However, prompt fission neutrons, emitted with a watt-energy spectrum [15], have energies up to 10 MeV and beyond.

The emission of prompt fission neutrons can be observed anywhere from nanoseconds to milliseconds after the incident pulse of high-energy photons [16]. To effectively exploit prompt signals for SNM detection, state-of-the-art detectors with spectroscopy capabilities and fast timing characteristics are needed. The *trans*-stilbene (diphenyl ethylene, C₁₄H₁₂) organic scintillation detector is one such detector that is best known for its timing characteristics and excellent pulse-shape-discrimination (PSD) capabilities [17]. Fast neutrons in *trans*-stilbene scintillators are detected through elastic scattering, i.e., proton recoil, whereas photons are detected through Compton scattering, i.e., electron recoil. The traditional charge-integration PSD method (Fig. 2) uses the difference in the shape of the scintillation pulses excited by recoil protons and recoil electrons to discriminate neutrons and photons. Additionally, *trans*-stilbene detectors are capable of neutron spectroscopy, which is useful in discriminating fission neutrons from other (γ, Xn) photoneutrons.

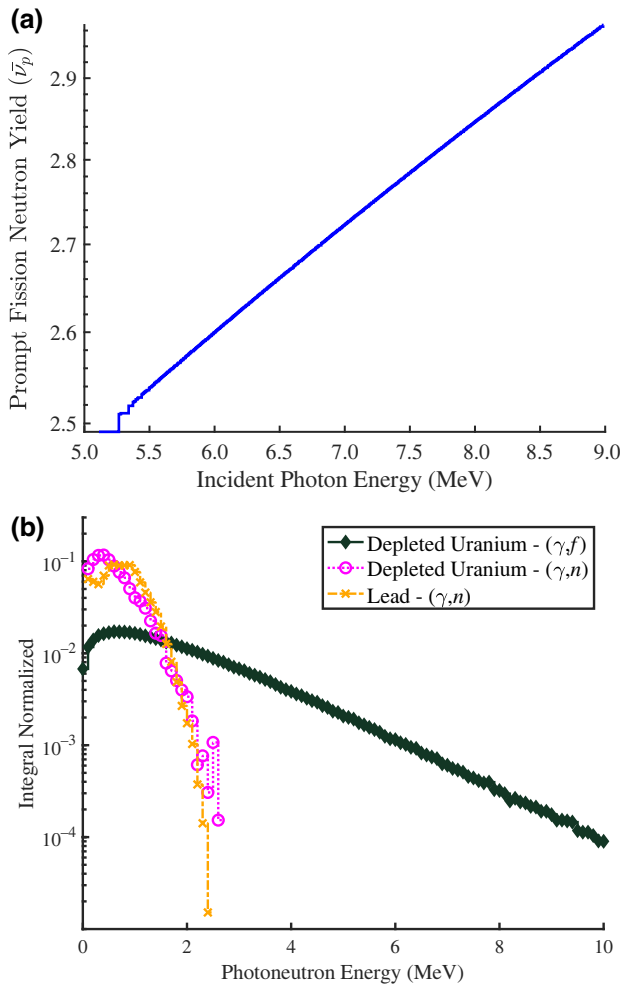


FIG. 1. MCNPX-PoliMi simulation of photonuclear reactions in depleted uranium and lead with 9-MeV endpoint bremsstrahlung photons: (a) prompt neutron yield per fission in depleted uranium and (b) energy spectrum of photoneutrons produced because of (γ, f) and (γ, n) photonuclear reactions.

III. EXPERIMENTAL SETUP AND DATA ANALYSIS

Our laboratory at the University of Michigan has a 9-MeV electron linac that is currently operating in pulsed mode with a pulse length of approximately $4 \mu\text{s}$ and a repetition rate of approximately 44 Hz. The bremsstrahlung radiation is collimated using a primary and secondary collimator. The primary collimator consists of lead backed with tungsten and has a beam spot size of 25 cm. The lead is 83 cm in diameter and 28 cm thick, whereas tungsten is 48 cm in diameter and 11 cm thick. The secondary collimator consists of lead, which is 74 cm square and 41 cm thick. The beam spot size is reduced from 25 to 5.08 cm at the exit of the secondary collimator.

Depleted uranium (DU), which is 99.7 wt % ^{238}U and 0.3 wt % ^{235}U , and lead targets are interrogated for an hour with the bremsstrahlung photons. The DU target is

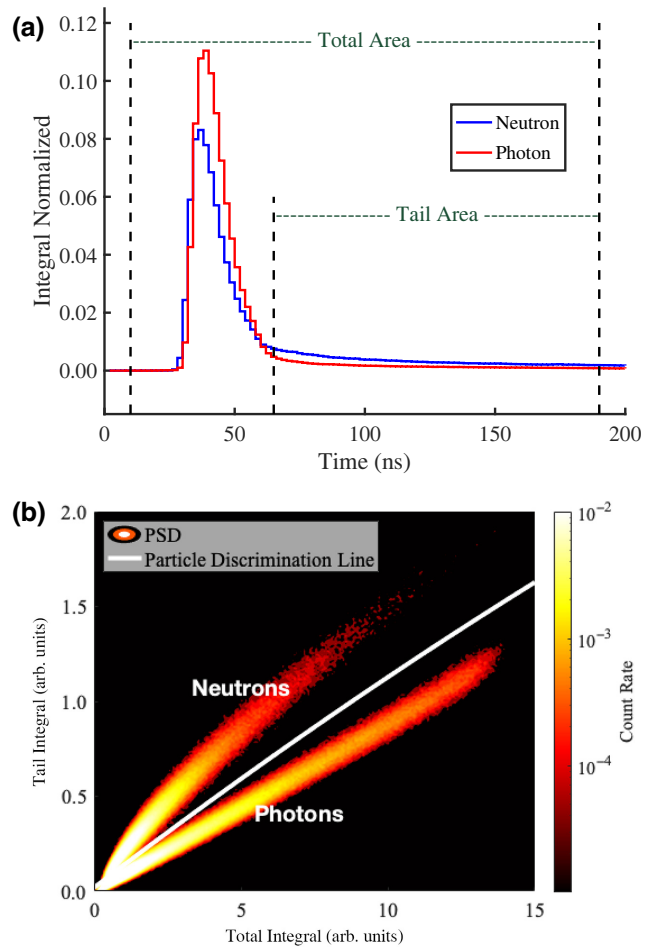


FIG. 2. (a) Traditional charge-integration method for PSD analysis and (b) measured ^{252}Cf PSD plot with a *trans*-stilbene detector 5.08 cm in length and 5.08 cm in diameter (70 keVee threshold).

a 5.23-cm cube, and the lead target has dimensions of $5.08 \times 5.08 \times 6.35 \text{ cm}^3$. Targets are placed in the beam 27 cm from the secondary collimator. At this location, the beam spot size is large enough to cover the entire surface area of the target, which is desired to maximize photoneutron production. The lead target produces neutrons through (γ, n) reactions, whereas the DU target produces neutrons through (γ, n) and (γ, f) reactions [18]. Lead interrogation provides a basis for which photoneutrons from an actinide, such as DU, can be compared to photoneutrons from a non-SNM target, such as lead. An active background measurement is also performed for an hour to account for photoneutrons produced in the collimator.

Four 5.08 cm in length and 5.08 cm in diameter *trans*-stilbene crystals coupled to a photomultiplier tube are used for the detection of fast neutrons. The photomultiplier tubes are 5.08 cm in diameter from ET Enterprises [19]. Scintillation pulses are digitized with a V1730 14-bits 500-MS/s digitizer from CAEN [20].

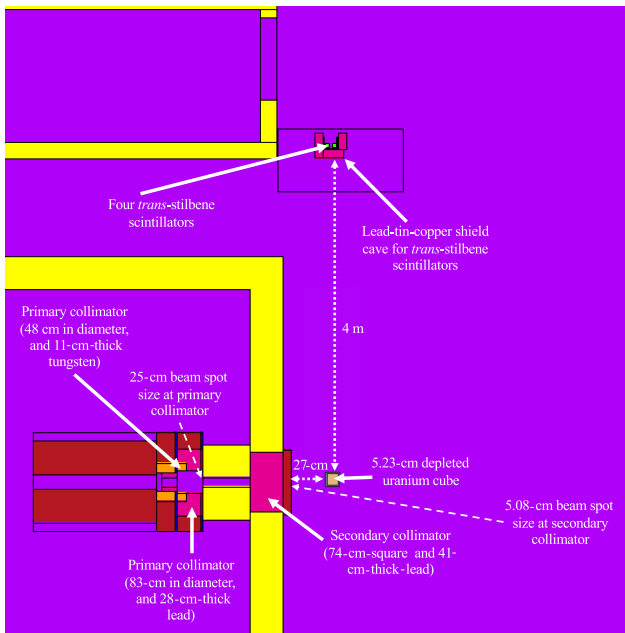


FIG. 3. Detailed geometry of the laboratory space defined in MCNPX-PoliMi (top-down view).

To reduce the bremsstrahlung photon flux incident on the detectors, a layered lead-tin-copper shield cave [21] is used. The front and sides of the cave consist of 10.16-cm-thick lead. There is 5.08-cm-thick lead at the top and bottom of the cave. Tin and copper are 0.64 cm thick and provide shielding to $K\alpha$ and $K\beta$ x-rays, which are produced in lead because of high-energy bremsstrahlung absorption [22]. Additionally, the detectors are placed perpendicular to the beam axis at 4 m from the front of the shield cave to the edge of the DU cube. This 4-m source-to-detector distance helps to reduce the probability of pile-up events, which is dependent on the radiation flux and voltage pulse width. The schematic of the experimental setup is shown in Fig. 3.

Time gating is performed to analyze detection events that arrive during the linac pulses. This time gating allows us to discriminate prompt photoneutrons from delayed fission neutrons, which are emitted through β decay of photofission fragments. Additionally, all data are processed with a lower light-output threshold of 0.28 MeVee and an upper threshold of 2.67 MeVee (MeV electron equivalent, i.e., the amount of light created by a photon-energy deposition in MeV). This light-output window corresponds to a proton-recoil energy of 1.66–6.85 MeV [Eq. (1)].

Scintillation events that arrive during the linac pulses are processed with an artificial neural network (ANN) system previously developed and demonstrated at the University of Michigan [23]. The ANN system consists of six feed-forward fully connected neural networks that work in conjunction to produce the desired classifications. The

ANN system is trained with high-confidence neutron and photon pulses acquired through a time-of-flight measurement with the ^{252}Cf source and has an overall classification accuracy of 99.5%. The ANN system identifies neutron, photon, and pile-up pulses and recovers neutron and photon information from pile-up events.

IV. MCNPX-PoliMi METHODOLOGY

The MCNPX-PoliMi simulation is performed in three steps using the ENDF/B-VII cross-section library: (1) electron simulation, (2) photonuclear simulation, and (3) detector-response simulation. For the electron simulation, the source particles are electrons with an energy of 10 MeV, and we tally bremsstrahlung photons exiting the secondary collimator. The 10-MeV energy of the electrons is based on a previous beam-quality measurement performed at the University of Michigan [24]. The bremsstrahlung spectrum obtained from the electron simulation is then used as a source to simulate photonuclear reactions in the DU cube. In the photonuclear simulation step, we tally photoneutrons exiting the edge of the DU cube that is facing the detectors. In step 3, the cosine- and energy-binned photoneutron distribution obtained from step 2 is used as a source. In this step, a particle-collision file is generated, which is then processed with the MCNPX-PoliMi postprocessing algorithm (MPPost) [25] to simulate the *trans*-stilbene detector's response. Birks formula,

$$L(E) = \int \frac{a}{1 + b(dE/dx)} dE, \quad (1)$$

is used in MPPost to convert energy deposited by neutrons into light output. In Eq. (1), $L(E)$ is the light output in MeVee, dE/dx is the particle-stopping power in the *trans*-stilbene detector, and a and b are the fitted coefficients obtained from Ref. [26].

The three-step simulation result is scaled to match the measured result using

$$R_{\text{scaled}} = N_{\text{MPPost}} B_{\text{photoneutron}} \times C_{\text{photons}} \frac{I_{\text{peak}}}{q_e} D, \quad (2)$$

where R_{scaled} is the scaled photoneutron count rate (counts per second), N_{MPPost} is the number of neutrons detected in the *trans*-stilbene detectors per photoneutron emitted from DU, $B_{\text{photoneutron}}$ is the number of photoneutrons leaving DU per bremsstrahlung photon incident on DU, C_{photons} is the number of bremsstrahlung photons leaving the secondary collimator per electron, I_{peak} is the peak linac current (97.2 mA), q_e is the elementary charge, and D is the linac duty factor (0.02%).

The average repetition rate of the linac is measured to be 44.15 Hz with a standard deviation of 0.09 Hz. This

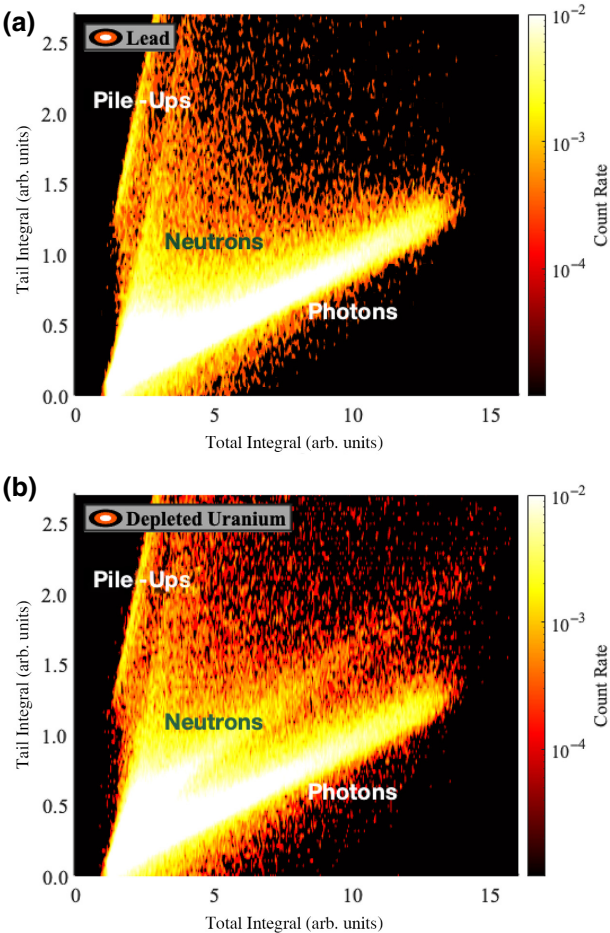


FIG. 4. Neutron and photon integrals before elimination of pile-up events: (a) lead and (b) depleted uranium.

deviation in the repetition rate is accounted for in the linac duty factor and the scaled photoneutron count rate.

V. RESULTS AND DISCUSSION

A. Measurement

Figures 4 and 5 show the detected pulse integrals for lead and depleted uranium interrogations before and after the elimination of pile-up events. Figure 4 shows that there are significant pile-up events that greatly deteriorate the neutron- and photon-detection capabilities of the *trans*-stilbene scintillators. Figure 5 shows the results after applying the developed ANN system. A good separation between neutrons and photons is observed; the ANN system successfully identifies the pile-up events.

Figure 6(a) shows the measured photoneutron light-output distributions for DU and lead. We observe a 5 times higher photoneutron count rate when the lead target is replaced with the DU target. Additionally, the measured light-output distribution for lead photoneutrons is much softer than the DU photoneutron light-output distribution.

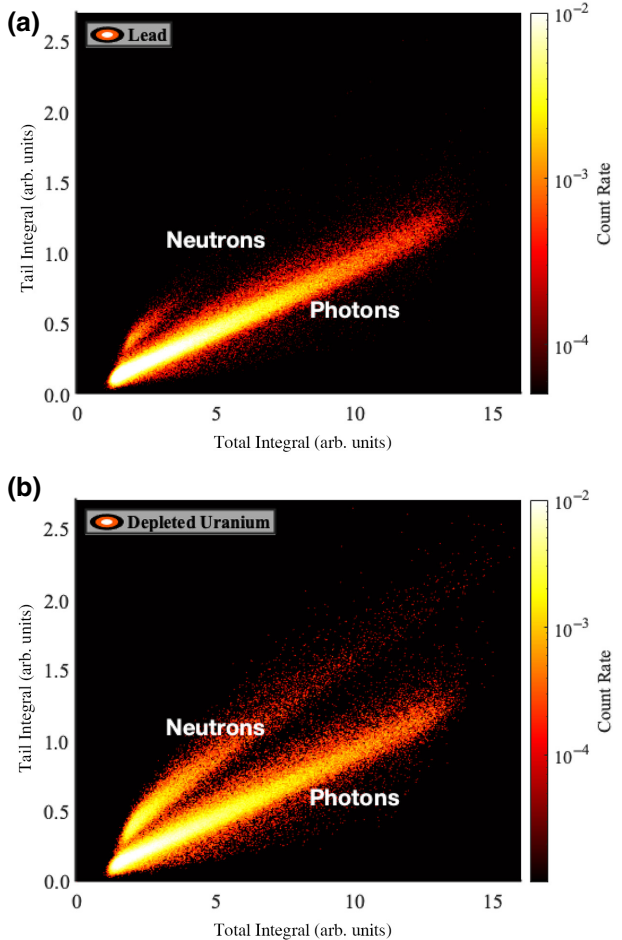


FIG. 5. Neutron and photon integrals without pile-up events: (a) lead and (b) depleted uranium.

This difference in the light-output distributions is due to the known difference in the photoneutron energy spectra. The DU photoneutrons are emitted with two energy spectra, i.e., (γ, n) and watt spectra, whereas lead photoneutrons are emitted with only the (γ, n) spectrum [Fig. 1(b)].

Without any pile-up recovery, the photoneutron count rate is 1.92 ± 0.07 counts per second for lead and 8.2 ± 0.1 counts per second for DU. After information is recovered from pile-up events, the count rate increases to 2.76 ± 0.08 counts per second for lead and 12.7 ± 0.1 counts per second for DU. We observe that the shape of the photoneutron light-output distributions remains unaffected after recovery of pile-up events [Fig. 6(b)]. This constant shape implies that pile-up recovery provides an efficiency boost of approximately 31% for neutron detection.

B. MCNPX-PoliMi

A passive ^{252}Cf measurement is performed to validate the MCNPX-PoliMi input geometry and *trans*-stilbene detector response. The ^{252}Cf spontaneous fission source is placed 4 m from the front of the lead-tin-copper shield

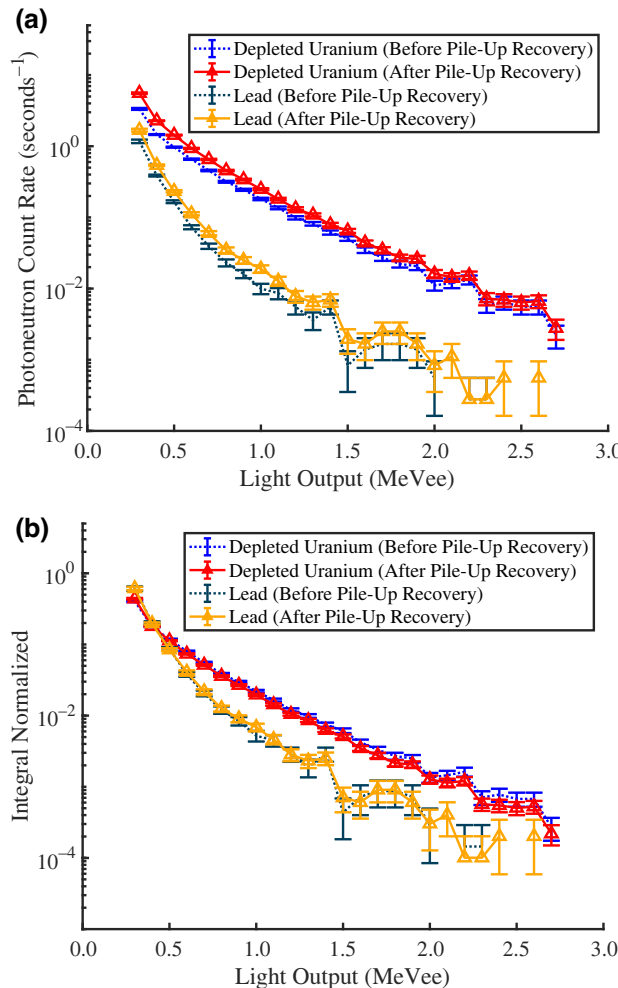


FIG. 6. Measured photoneutron light-output distributions for lead and depleted uranium: (a) absolute comparison and (b) integral normalized comparison. (Active background is subtracted from each distribution. Error bars are from Poisson counting statistics and are represented within one standard deviation.)

cave, which is the same as the DU-to-shielding distance. The measured data are analyzed with the ANN system.

Figure 7 shows the measured and simulated neutron light-output distributions. The simulated and measured neutron count rates agree within $8.6\% \pm 0.8\%$. The measured count rates before and after recovery of pile-up events are statistically identical, which is expected due to the low activity of the ^{252}Cf source and the large source-to-detector distance (>4 m). The discrepancy between the measured and simulated rates is primarily due to the source-strength uncertainty that is used to scale MPPost results. The passive ^{252}Cf result demonstrates our ability to accurately simulate the *trans*-stilbene detector response with the MCNPX-PoliMi transport code.

Figure 8 shows the measured and simulated photoneutron light-output distributions for DU. For a light-output window of 0.28–0.60 MeVee, the simulation is found to

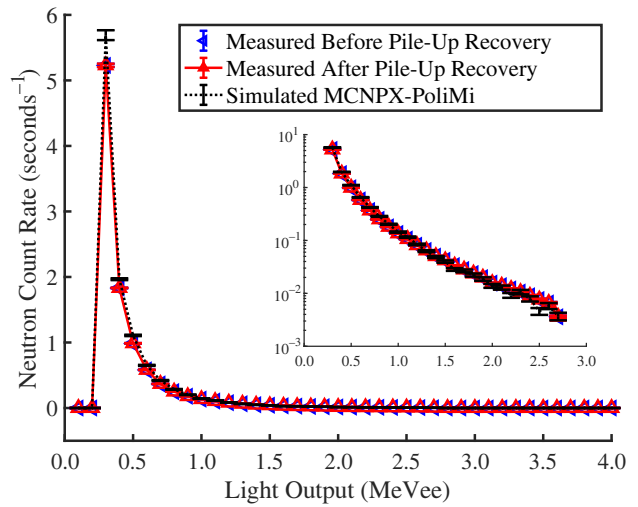


FIG. 7. Measured and simulated neutron light-output distributions from a ^{252}Cf spontaneous fission source (inset shows data on a logarithmic y axis).

overestimate the measured result. This overestimation is due to the information that is lost to unrecoverable pile-up events (29.5% of the collected data are eliminated). Nearly 75% of these unrecoverable pile-up events are voltage signals that have a small amplitude (less than 0.60 MeVee) and a poor voltage signal-to-noise ratio. The developed MCNPX-PoliMi framework does not simulate the pulse pile-up effect in *trans*-stilbene scintillators.

For a light-output window of 0.60–2.67 MeVee, the simulation is found to underpredict the measured result by an

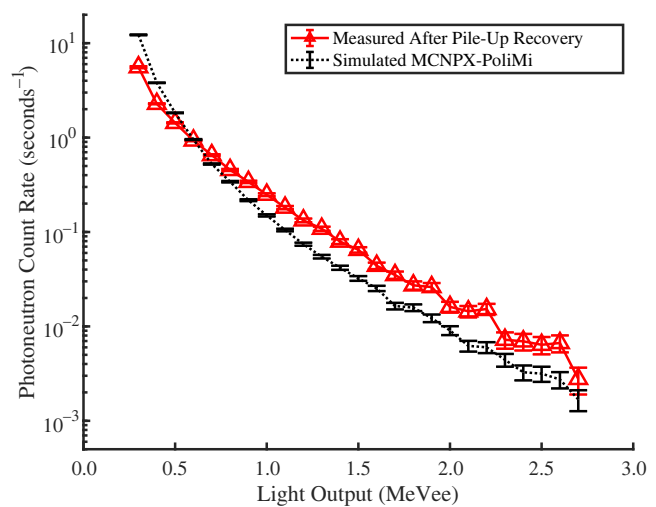


FIG. 8. Measured and simulated photoneutron light-output distributions for depleted uranium. (Represented error bars are within one standard deviation.)

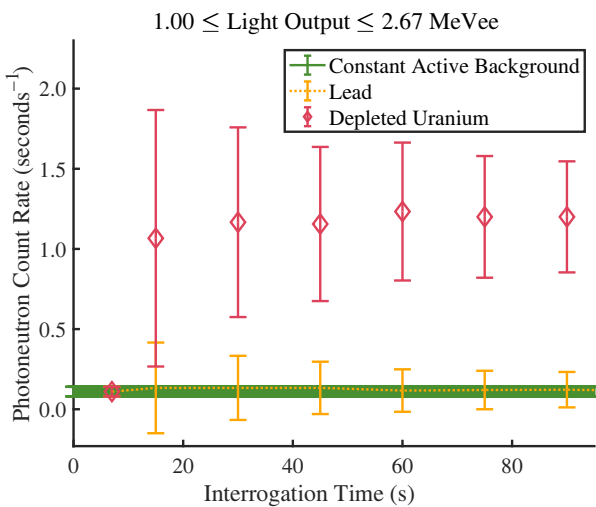


FIG. 9. Photoneutron count rates in depleted uranium and lead as a function of interrogation time. (Error bars are from Poisson counting statistics and are represented within three standard deviations.)

average of $33.3\% \pm 1.2\%$. The underprediction of simulation versus experiment in our result confirms the previously reported underprediction when using ENDF/B-VII photonuclear cross-section data for uranium [27,28].

Frankl and Macián-Juan [29] performed a photonuclear benchmark study on natural uranium with MCNPX using ENDF/B-VII cross-section libraries. In the benchmark study, the MCNPX results are compared to measured results that were obtained by Barber and George in 1959 [30]. The simulation was found to underpredict the measured count rate by $8.7\% \pm 15.1\%$ for a 0.98-cm-thick natural uranium target interrogated with bremsstrahlung photons produced by 11.5-MeV electrons. Here, the DU cube is 5.23 cm and is interrogated with bremsstrahlung photons produced by 9-MeV electrons. We observe an underestimation of $33.3\% \pm 1.2\%$ in the simulated photoneutron count rate. The underprediction of simulation versus experiment is consistent with the Frankl and Macián-Juan result, and therefore, we can be confident that the ANN system is correctly recovering information from pile-up events.

C. Time to detection

The observed difference (Fig. 6) in the photoneutron light-output distributions of lead and DU can be exploited to discriminate SNMs from non-SNM neutron-producing targets. A light-output window of 1.00–2.67 MeVee is selected. Using Eq. (1), the light-output window corresponds to a proton-recoil energy of 3.68–6.85 MeV. This energy is sufficiently high to eliminate (γ, n) photoneutrons. Only prompt photofission neutrons are energetic enough to deposit such high energy in the scintillator, and therefore, false-positive alarms can be reduced in the field

by counting neutrons that deposit energies between 3.68 and 6.85 MeV. False positives are of great concern in cargo-scanning applications, wherein high-energy-photon interrogation systems are used for SNM detection.

Figure 9 shows the photoneutron count rate in the 1.00–2.67 MeVee light-output window as a function of interrogation time. We observe that the photoneutron count rate in the presence of DU is greater than the active background count rate by three standard deviations during the first 30 s of interrogation. This result demonstrates that a SNM surrogate may be flagged in the field in as quickly as 30 s, which is well within the American National Standard Institute (ANSI) standard inspection times for clearing cargo packages [31].

VI. CONCLUSIONS

We present experimental results that demonstrate the detection of prompt photofission neutrons from a depleted uranium cube. These neutrons are detected with *trans*-stilbene organic scintillators, which are state-of-the-art detectors that are spectroscopy capable. The intense bremsstrahlung photons create pulse pile-up, which deteriorates the particle-discrimination capabilities of the *trans*-stilbene scintillator. To address the pulse pile-up issue, we apply neural-network-based digital processing to scintillation pulses. The information recovered from neutron pile-up events provides an efficiency boost of approximately 31% to the interrogation system.

We exploit the difference in the measured photoneutron light-output distributions of lead and DU to discriminate between (γ, n) and photofission neutrons. By selecting a light-output window of 1.00–2.67 MeVee, we demonstrate that a SNM surrogate, such as depleted uranium, can be detected in as little as 30 s and differentiated from a non-SNM material, such as lead.

We also present a framework that can be used to simulate active interrogation experiments with the MCNPX-PoliMi transport code. The developed framework is validated with measured results with a ^{252}Cf source. In the photonuclear experiments, for a light-output window of 0.60–2.67 MeVee, the simulated result is found to underpredict the measured result by $33.3\% \pm 1.2\%$. This result is expected due to the known underprediction in the photonuclear cross-section data for uranium. Future work is needed to improve the photonuclear cross-section data and uncertainties. The validated MCNPX-PoliMi framework can be used to study the response of the active interrogation systems when the SNM is surrounded by shielding materials.

ACKNOWLEDGMENTS

This work is supported by the U.S. Department of Homeland Security, Countering Weapons of Mass

Destruction Office, Academic Research Initiative, under Grant No. 2016-DN-077-ARI106.

A.J.J. wrote the main manuscript, conducted the formal analysis, and aided in the conceptualization. T.E.M. and C.A.M. assisted in data collection, data analysis, and review and editing of the manuscript. O.V.P. aided in the simulation and review and editing of the manuscript. H.S.K. and D.D.W. assisted in the development of software and review and editing of the manuscript. S.D.C. and S.A.P. conceived the initial idea, acquired funding, aided in the conceptualization, and reviewed and edited the manuscript.

-
- [1] T. Gozani, *Active Nondestructive Assay of Nuclear Materials* (U.S. Nuclear Regulatory Commission, Washington, D.C., 1981). NUREG/CR-0602.
- [2] J. Stevenson, T. Gozani, M. Elsalim, C. Condron, and C. Brown, Linac based photofission inspection system employing novel detection concepts, *Nucl. Instrum. Methods Phys. Res., Sect. A* **652**, 124 (2011).
- [3] B. W. Blackburn, J. L. Jones, C. E. Moss, J. T. Mihalczo, A. W. Hunt, F. Harmon, S. M. Watson, and J. T. Johnson, Utilization of actively-induced, prompt radiation emission for nonproliferation applications, *Nucl. Instrum. Methods Phys. Res., Sect. B* **261**, 341 (2007).
- [4] S. D. Clarke, S. A. Pozzi, S. J. Thompson, and A. W. Hunt, in *2008 Symposium on Radiation Measurements and Applications* (Berkely, California, U.S.A., 2008).
- [5] A. Sari, F. Carrel, F. Lainé, and A. Lyoussi, Neutron interrogation of actinides with a 17 MeV electron accelerator and first results from photon and neutron interrogation non-simultaneous measurements combination, *Nucl. Instrum. Methods Phys. Res., Sect. B* **312**, 30 (2013).
- [6] J. M. Mueller, M. W. Ahmed, and H. R. Weller, A novel method to assay special nuclear materials by measuring prompt neutrons from polarized photofission, *Nucl. Instrum. Methods Phys. Res., Sect. A* **754**, 57 (2014).
- [7] J. M. Mueller, M. W. Ahmed, A. Kafkarkou, D. P. Kendellen, M. H. Sikora, M. C. Spraker, H. R. Weller, and W. R. Zimmerman, Tests of a novel method to assay SNM using polarized photofission and its sensitivity in the presence of shielding, *Nucl. Instrum. Methods Phys. Res., Sect. A* **776**, 107 (2015).
- [8] K. W. Chin, H. Sagara, and C. Y. Han, Application of photofission reaction to identify high-enriched uranium by bremsstrahlung photons, *Ann. Nucl. Energy* **158**, 108295 (2021).
- [9] R. Kimura, H. Sagara, and S. Chiba, Principle validation of nuclear fuel material isotopic composition measurement method based on photofission reactions, *J. Nucl. Sci. Technol.* **53**, 1978 (2016).
- [10] S. Van Liew, W. Bertozzi, N. D’Olympia, W. A. Franklin, S. E. Korbl, R. J. Ledoux, and C. M. Wilson, Identification and imaging of special nuclear materials and contraband using active x-ray interrogation, *Phys. Procedia* **90**, 313 (2017).
- [11] A. Danagoulian, W. Bertozzi, C. L. Hicks, A. v. Klimenko, S. E. Korbl, R. J. Ledoux, and C. M. Wilson, in *2010 IEEE International Conference on Technologies for Homeland Security, HST 2010* (2010), pp. 379.
- [12] C. A. Meert, A. T. Macdonald, A. J. Jinia, W. M. Steinberger, S. D. Clarke, and S. A. Pozzi, Photoneutron detection in active interrogation scenarios using small organic scintillators, *IEEE Trans. Nucl. Sci.* **1**, 9499 (2022).
- [13] S. A. Pozzi, E. Padovani, and M. Marseguerra, MCNP-PoliMi: A Monte-Carlo code for correlation measurements, *Nucl. Instrum. Methods Phys. Res., Sect. B* **513**, 550 (2003).
- [14] J. T. Caldwell, E. J. Dowdy, R. A. Alvarez, B. L. Berman, and P. Meyer, Experimental determination of photofission neutron multiplicities for ^{235}U , ^{236}U , ^{238}U , and ^{232}Th using monoenergetic photons, *Nucl. Sci. Eng.* **73**, 153 (1980).
- [15] N. V. Kornilov, Verification of the ^{252}Cf standard in the energy range 2–20 MeV. (2015).
- [16] R. C. Runkle, D. L. Chichester, and S. J. Thompson, Rattling nucleons: New developments in active interrogation of special nuclear material, *Nucl. Instrum. Methods Phys. Res., Sect. A* **663**, 75 (2012).
- [17] J. B. Birks, *The Theory and Practice of Scintillation Counting* (Pergamon Press, New York, 1964).
- [18] M. B. Chadwick, *et al.*, ENDF/B-VII.0: Next generation evaluated nuclear data library for nuclear science and technology, *Nucl. Data Sheets* **107**, 2931 (2006).
- [19] ET Enterprises, ET Enterprises 51 Mm (2") Photomultiplier 9214B Series Data Sheet, <https://et-enterprises.com/products/photomultipliers/product/p9214b-series>
- [20] CAEN, CAEN V1730/V1730S 16/8 Channel 14 Bit 500 MS/s Digitizer, <https://www.caen.it/products/v1730/>
- [21] N. Kleedtke, M. Hua, and S. Pozzi, Genetic algorithm optimization of tin–copper graded shielding for improved plutonium safeguards measurements, *Nucl. Instrum. Methods Phys. Res., Sect. B* **988**, 164877 (2021).
- [22] R. D. Deslattes, E. G. Kessler, Jr., P. Indelicato, L. de Billy, E. Lindroth, and J. Anton, X-ray transition energies: New approach to a comprehensive evaluation, *Rev. Mod. Phys.* **75**, 35 (2003).
- [23] A. J. Jinia, T. E. Maurer, C. A. Meert, M. Y. Hua, S. D. Clarke, H. S. Kim, D. D. Wentzloff, and S. A. Pozzi, An artificial neural network system for photon-based active interrogation applications, *IEEE Access* **9**, 1 (2021).
- [24] N. H. Ba Sunbul, Dissertation at the University of Michigan, 2022.
- [25] E. C. Miller, S. D. Clarke, S. A. Pozzi, and E. Padovani, MCNPX-PoliMi post-processing algorithm for detector response simulation, *J. Nucl. Mater. Manage.* **40**, 34 (2012).
- [26] T. H. Shin, P. L. Feng, J. S. Carlson, S. D. Clarke, and S. A. Pozzi, Measured neutron light-output response for trans-stilbene and small-molecule organic glass scintillators, *Nucl. Instrum. Methods Phys. Res., Sect. A* **939**, 36 (2019).
- [27] A. Sari, Characterization of photoneutron fluxes emitted by electron accelerators in the 4–20 MeV range using Monte Carlo codes: A critical review, *Appl. Radiat. Isot.* **191**, 110506 (2023).

- [28] V. V. Varlamov, Reliability of photonuclear data: Various experiments and evaluations, *Phys. Part. Nucl.* **50**, 637 (2019).
- [29] M. Frankl and R. Macián-Juan, Photonuclear benchmarks of C, Al, Cu, Ta, Pb, and U from the ENDF/B-VII cross-section library ENDF7U using MCNPX, *Nucl. Sci. Eng.* **183**, 135 (2016).
- [30] W. C. Barber and W. D. George, Neutron yields from targets bombarded by electrons, *Phys. Rev.* **116**, 1551 (1959).
- [31] American National Standard Minimum Performance Criteria for Active Interrogation Systems Used for Homeland Security, ANSI N42.41-2007 1 (2008).